LHCb-PUB-2019-006.
November 5, 2019

Description of Light Guidance in Dual Clad Scintillating Fibres for the LHCb SciFi Tracker

M. Bieker[1], R. Ekelhof[1], R. Manderfeld[1].

[1] *Fakultät Physik, Technische Universität Dortmund, Dortmund, Germany*

Abstract

During the LHCb upgrade in 2019/2020, a new detector element will be installed that uses scintillating fibres (SciFi) to detect particle tracks, the so-called SciFi Tracker. To predict its performance, a single fibre simulation has previously been developed with the GEANT4 toolkit. The simulation results are compared to measurements in order to tune the simulation parameters and gain an understanding of the underlying fibre properties. This note presents the relevant information obtained so far and new findings concerning the reflection losses in scintillating fibres.

Contents

1 Introduction

The Scintillating Fibre Tracker (SciFi Tracker) is a major component of the LHCb Upgrade, to be installed in 2019/20. It is made from thin fibres which are read out by multichannel silicon photomultipliers (SiPMs). The fibres are 2.5 m long and have a diameter of 250 µm which enables a spatial resolution of less than 100 µm.
An important aspect of the detector is the light guidance and especially the transmission loss in the fibres. For every ionizing particle, only a handful of photons are expected to reach the SiPMs at the end of the fibres, so it is important to minimise the number of photons lost inside the fibres. The total attenuation of light along the fibre is a combination of absorption, scattering and boundary effects at the material interfaces inside the fibre. It is highly dependent on the photon wavelength and angle, as well as on the amount of radiation experienced by the fibre and its age. These losses scale differently with the angle of the photon path to the fibre axis and can therefore be analysed separately.
During the detector lifetime the fibres close to the beam pipe are expected to be exposed to a high radiation dose (30 kGy), which damages the fibres and worsens their ability to transmit light.
A single fibre simulation has been developed to predict the performance of the detector and study fibre behaviour. Studies comparing measurements to results obtained through this simulation are used to improve the simulation parameters and our understanding of the underlying mechanisms.
This document describes the behaviour of the scintillating fibres that is obtained from comparison between the simulation and the measurements. Chapter 2 reiterates important fibre properties. First, the mechanisms responsible for photon creation and capture are mentioned, as well as the fibre geometry. The transmission losses are introduced in this chapter as well. Chapter 3 gives a brief overview of the single fibre simulation used to obtain the results presented in this document. In chapter 4, the different attenuation mechanisms are explained and the simulation results are compared to the measurements in order to tune the simulation parameters. Finally, chapter 5 summarises the contents of this document.

2 Theory of Light Guidance in Scintillating Fibres

2.1 Photon Creation

The scintillating fibres used in the SciFi Tracker are of type SCSF-78MJ manufactured by Kuraray. They consist of a polystyrene core with a radius of 110 µm, which functions as the active material where photons are created from deposited energy of traversing ionizing particles. Energy deposited by these particles excite the π-electrons of the molecule, which quickly decay back to the ground state, giving off a photon in the process.
To improve the low quantum yield of pure polystyrene, a dye called p-Terphenyl (PT) is added ($\sim 1\,\%$ by weight). Energy transfer to the dye occurs by means of a non-radiative dipole-dipole transmission, the so-called Förster transfer. Photons emitted by the PT

have an attenuation length of about 1 m. Through the addition of a wavelength-shifter ($\sim$ 0.05 % by weight), the attenuation length can be raised significantly. In order for the wavelength-shifter to be effective, its absorption spectrum has to closely match the emission spectrum of PT, as shown in Figure 1. Additionally the Stokes shift between the absorption and emission spectra of the wavelength shifter needs to be sufficiently large to suppress reabsorption. The fibres used in the LHCb detector utilize tetraphenyl-butadiene (TPB), which raises the attenuation length to an average of 3.5 m. [1, 2]

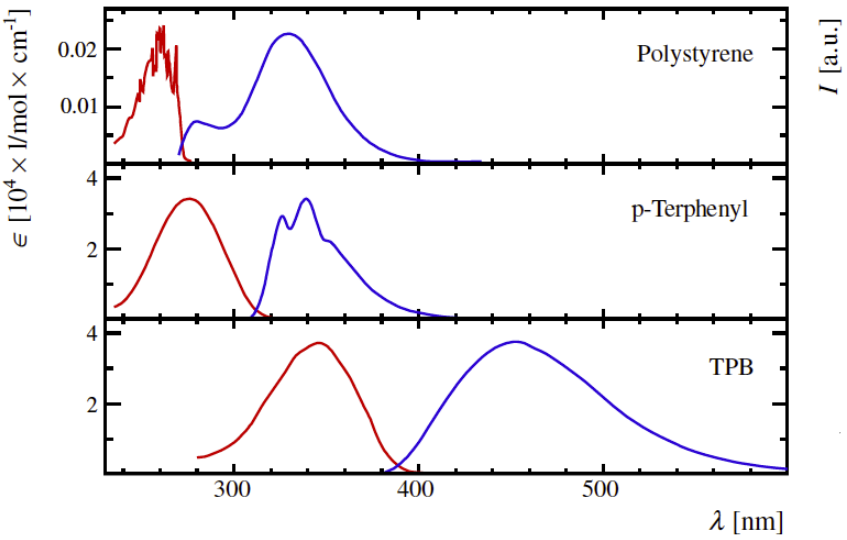

Figure 1: Absorption (red) and emission (blue) spectra of polystyrene and the two added dyes p-Terphenyl and TPB. Figure taken from Ref. [3], modified.

2.2 Photon Collection

The core of the scintillating fibres is surrounded by two claddings, which serve the purpose of guiding the light created within the fibre core to the photodetectors at the end of the fibre. The light is held in the fibre via total internal reflection at the material interfaces. For this reason, the indices of reflection of the claddings are smaller than that of the core. The individual cladding thickness is about 3 % of the total fibre diameter, which is 250 µm in this case. Figure 2 shows the schematic structure of a dual-clad fibre. The refractive indices of the different materials are, however, dependent on the wavelength λ of the photon. To calculate their precise values, a Sellmeier equation of the form

$$n(\lambda) = \sqrt{1 + \frac{a\lambda^2}{\lambda^2 - b}} \tag{1}$$

was fitted to experimental data for the various materials in the scope of Ref. [3]. The parameters a and b are listed in Tab. 1 in the appendix.

In the following the angle of the photons with respect to the fibre axis while inside the fibre will be referred to as the inner angle θ. Photons leaving the fibre at the end faces are refracted and observed under an outer angle θ'. The maximum angle of reflection can be calculated using Snells law. The photons with an inner angle θ of more than about 21° with respect to the fibre axis leave the core material and enter the first cladding. The maximum angle, under which the photons are totally reflected at the cladding-cladding interface is about 27°. For larger angles, the photons leave the fibre entirely. From this value, the trapping efficiency for isotropically emitted photons is estimated to be about 11 %. It is important to note that this number is only valid for photons that cross the fibre axis. Most photons, however, have a certain distance r_{min} to the fibre axis, which causes their paths to follow a helical shape. These skew photon paths allow photons with the same angle to the fibre axis (inner angle) to have differing angles with respect to the core-cladding interface (interface angle). The interface angle θ_{refl} is relevant for total internal reflection and can be calculated with

$$\theta_{\text{refl}} = \arcsin\left(\sqrt{1 - \frac{r_{\text{min}}^2}{r_{\text{core}}^2}}\sin\theta\right) , \tag{2}$$

where r_{core} is the radius of the fibre core [4]. Using a simulation, the trapping efficiency is determined to be roughly 18 % if skew photons are included.

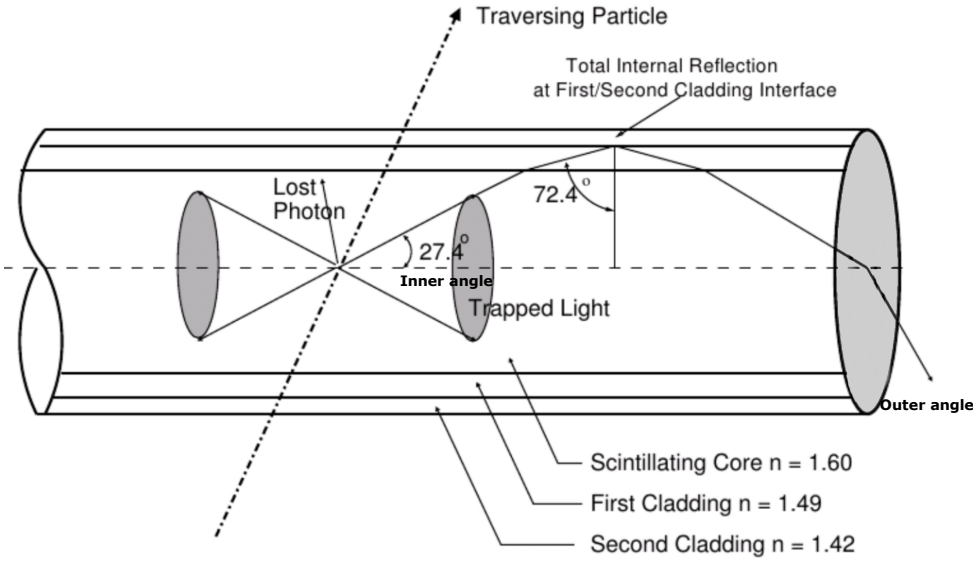

Figure 2: Schematic structure of a dual-clad scintillating fibre. [1].

2.3 Light Guidance and Transmission Losses

When the light travels through the fibre, photons can be lost due to several loss mechanisms. The losses can be divided into two categories: On the one hand, there are attenuation

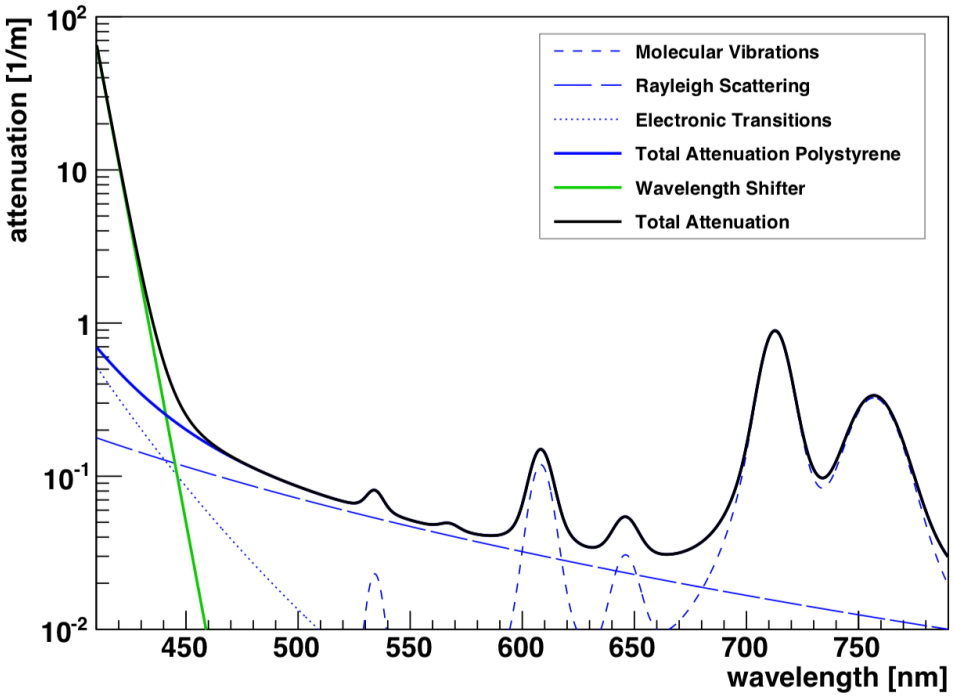

Figure 3: Wavelength-dependent attenuation coefficient of scintillating fibres and its components. Image taken from Ref. [5], with data taken from Ref. [3].

sources that scale with the path length L of the photons inside the fibre. The light intensity I decreases exponentially as a function of L

$$I = I_0 \cdot e^{-aL}\,, \tag{3}$$

where I_0 is the initial light intensity and a is the base attenuation coefficient of the fibre material. As shown in Fig. 3, the base attenuation coefficient a is the sum of multiple components, including Rayleigh scattering, electronic transitions, molecular vibrations, absorption of the wavelength shifter, as well as reflection losses at the interfaces.
Irradiation causes the creation of additional absorption centres, which increase the attenuation coefficient in the core. Additionally, the attenuation coefficient of fibres has been observed to increase with time, even without irradiation. This is referred to as natural fibre ageing.
As mentioned above, these loss mechanisms scale with the path length L in the medium, which is a function of the inner angle θ and the distance to the excitation point x:

$$L(x, \theta) = \frac{x}{\cos\theta}\,. \tag{4}$$

They are further elaborated in Ch. 4.1.
On the other hand, there are reflection losses that scale with the number of reflections N. These are due to imperfections at the material interfaces, which have a chance to scatter

photons. The number of reflections depends on the angle θ and the smallest distance of the photon path to the fibre axis r_{min}. It is given by

$$N(x, \theta) = \frac{x \tan \theta}{2\sqrt{r_{\text{core}}^2 - r_{\text{min}}^2}} \,. \tag{5}$$

While the path length L stays constant with varying values of r_{min}, the number of reflections increases drastically for skew photons, which causes them to be more attenuated. The probability to loose a photon at a single reflection is called the reflection loss coefficient ϵ. Equations 4 and 5 are only valid for photons moving exclusively in the fibre core. For photons entering the cladding, a new model has been developed using simple geometric relations to describe their path lengths in the different media, the number of reflections, and the interface angle with respect to the cladding-cladding interface [4]. The resulting formulas are listed in the appendix in Ch. 6.2.
The total attenuation factor A is the product of the base attenuation A_{base} and attenuation through reflection losses A_{refl}. The base attenuation can be expressed with Eq. 3 and 4:

$$A_{\text{base}} = \exp(-aL(x, \theta)) = \exp\left(\frac{-ax}{\cos \theta}\right) \,. \tag{6}$$

Attenuation caused by reflection losses can be expressed as

$$A_{\text{refl}} = (1 - \epsilon)^{N(x,\theta)} \approx \exp\left(\frac{-x\epsilon \tan \theta}{2\sqrt{r_{\text{core}}^2 - r_{\text{min}}^2}}\right) \,, \tag{7}$$

with an approximation that is valid for $\epsilon \ll 1$, which is satisfied with ϵ being in the order of 5×10^{-5}. This gives the total intensity as

$$I(x, \theta) = I_0 \exp\left(-x\left(\frac{a}{\cos \theta} + \frac{\epsilon \tan \theta}{2\sqrt{r_{\text{core}}^2 - r_{\text{min}}^2}}\right)\right) \,. \tag{8}$$

The part in the parenthesis multiplied by x is the effective attenuation coefficient a_{eff} (the inverse of the attenuation length). This value can be determined via measurements. For measurements taken at an angle of 0°, reflection losses disappear and the base attenuation coefficient a can be examined.

3 Single Fibre Simulation

To assess the performance of the future detector and enable the analysis of underlying fibre processes that would not be measurable in actual measurements, the working group at TU Dortmund has developed a single fibre simulation with the GEANT4 toolkit. [3] It is written in the C++ programming language and utilizes the ROOT data analysis framework to save data in ROOT TTree structures. The fibre can be subdivided into multiple sections of equal length, each with a specific irradiation dose. This way, a varied

radiation dose profile along the fibre can be studied. A detector volume is placed at one end of the fibre and a mirror is placed at the opposing end. All photons touching the detector volume are saved in a separate `TTree` called `DetectedPhotons`.

The entire fibre is placed in a vacuum, which allows additional internal reflections at the outermost fibre boundary. At the start of the simulation, parameter files have to be provided to the program, setting the different simulation properties. This enables flexible use of the fibre simulation. An exhaustive list of all input parameters provided with these files, as well as the recorded data of the individual photons, can be found in Ref. [6]. The necessary parameter files to run the simulation can be found in the appendix (Ch. 6.3). For the simulation studies shown in this document, the fibre is exited at 24 different positions, with each excitation occurring in a separate simulation. Instead of exciting the fibre with an ionizing particle, 200,000 photons are created directly in the fibre core with a random direction of travel and a wavelength according to the emission spectrum of p-Terphenyl. For every excitation point, the simulation is performed a total of 50 times, each with a different random seed in order to gain more data.

Reflection losses are not implemented in the GEANT4 simulation directly but are instead added in the analysis after the simulation is already completed. This allows to study the effects of different reflection loss coefficients without the need to redo the entire GEANT4 simulation, which can be time consuming. For every single photon, a probability to remain in the fibre is calculated from its wavelength, interface angle and number of reflections on the respective interface. A random number is drawn to determine whether the photon is detected or discarded.

4 Comparison of Measurements and Simulation

There are two general loss mechanisms: base attenuation in the materials and reflection losses at the material interfaces. Both of these have different angular dependencies, which makes it possible to separately analyse them with angle-dependent measurements.
The reflection losses have been observed to contribute significantly to the total attenuation observed in the fibres. Therefore, to get accurate results from the simulation, the exact nature of these reflection losses has to be understood.

4.1 Base Attenuation

The base attenuation coefficient a is the sum of multiple components: Rayleigh scattering a_r, electronic transitions a_e, molecular vibrations a_v, absorption by the wavelength-shifter a_wls and imperfections in the fibre a_i.
A function describing the attenuation coefficient of fibres has been described in detail in Ref. [3], which is why it is only mentioned briefly in this document.
The function was fitted to literature values and fibre measurements performed at CERN,

yielding the 22 necessary parameters for a complete description. These measurements were performed on so-called pre-series fibres. In the time since these measurements were performed, however, the fibre quality has improved in main-series fibres, which lowers the attenuation due to the fibre imperfections a_i. Measurements of main-series fibres performed in Ref. [4] lead to a reduction of this additional parameter from $4.65 \times 10^{-2}\,\mathrm{m}^{-1}$ to $1 \times 10^{-2}\,\mathrm{m}^{-1}$. The attenuation determined from measurements and the function used to describe it in simulation are shown in Fig. 4.

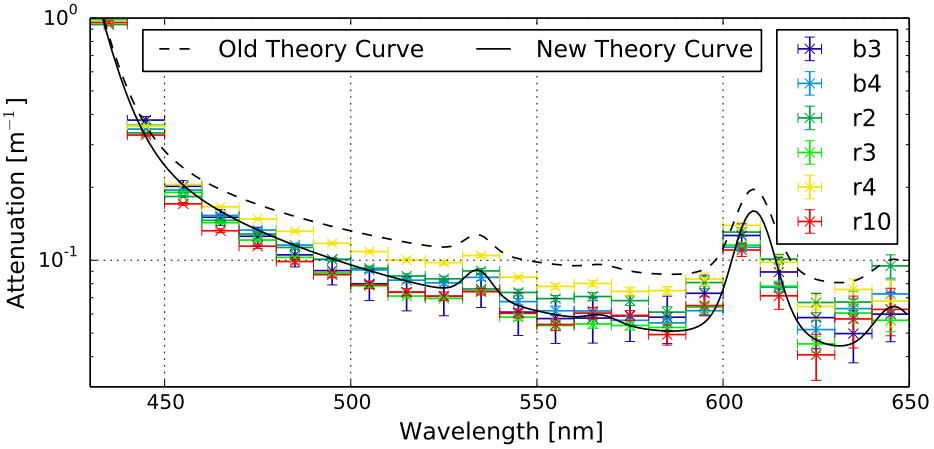

Figure 4: Wavelength-dependent attenuation coefficient obtained from measurements and the function describing the attenuation coefficient in simulation. The dashed line shows the function fitted to pre-series fibres and the solid line shows the corrected function for main-series fibres. Multiple measurements are shown in different colors. [4]

Irradiation causes the creation of additional absorption centres, which increases the attenuation coefficient in the core. Two different models are proposed, one following a power law and one assuming a linear dependency. The attenuation coefficient caused by radiation damage a_r is given by:

$$a_{\mathrm{r,pow}} = 0.4 \cdot D^{0.8} \cdot e^{-3.01\times10^{-2}(\lambda-450)}\,,$$
$$a_{\mathrm{r,lin}} = 0.38 \cdot D \cdot e^{-3.01\times10^{-2}(\lambda-450)}\,,$$

where D is the radiation dose in kGy and λ is the wavelength in nm. [5]

Additionally, the attenuation coefficient of fibres has been observed to increase with time, even without irradiation. The reason for this is assumed to be the slow oxidation of the polystyrene core, which decreases the transparency of the fibre material. The extent of the damage is not well known at this time, but the decrease in attenuation length is determined from repeated attenuation length measurements over the course of 30 months to be about 1.4 % per year. Since the detector is planned to be in operation for 10 years, the damage sustained through the natural ageing process would be significant. For now it

is unclear, whether this ageing process also occurs in the fibres that have been processed into the detector modules and are surrounded by the epoxy glue. [2]

4.2 Reflection Losses

If the fibre is placed in air, as in the measurements that were performed for the results shown in this document, total internal reflection could theoretically occur at the fibre-air boundary. Similarly, the simulation places the fibre in a vacuum to obtain comparable results. The measurements discussed in this note are performed and described in Ref. [4]. The results of measurement and simulation do not match, however, as the similar refractive indices of air and vacuum would indicate. As the black line in Fig. 5 shows, the simulation shows significantly more photons at higher angles than the measurement. A better match is achieved when photons that interact with the interface of outer cladding and the surrounding medium are eliminated entirely, indicating that photons entering the second cladding are lost in the actual fibre. This is depicted as the grey curve.
Preliminary measurements have been performed to get a rough value of the reflection loss coefficient at the core-cladding and cladding-cladding interfaces. First estimates put it at a constant value of 5×10^{-5} [7], but it is now assumed to be dependent on photon wavelength and the angle of reflection. In addition, it is assumed that the reflection losses are different for the various interfaces.
First, a value for the reflection loss coefficient at the core-cladding interface ϵ_{co} is determined. For this reason, the influence of cladding photons on the results has to be minimised. From simulation, the number of cladding photons can be determined as a fraction of all photons for different inner angles. This is shown in Fig. 6. At inner angles below 20°, all photons move exclusively in the core. Cladding photons peak at an angle of 27°, where they are in the majority with 70 %.
Since the inner angle is not actually the angle relevant for total internal reflection, an average value of the interface angle is determined for all inner angles from simulation. This is done for core and cladding photons separately and the results are shown superimposed in Fig. 7. For cladding photons, the interface angle measures the angle relative to the cladding-cladding interface as opposed to the core-cladding interface, where they are refracted. For inner angles below 20°, the average interface angle is proportional to the inner angle.
From measurements, the total attenuation coefficient can be determined at every angle. It is obtained from a fit of an exponential function (Eq. 3) to the intensities at different excitation positions as shown in Fig. 8. From Eq. 8 follows that

$$a_{\mathrm{tot}} = \frac{a}{\cos\theta} + \frac{\epsilon \tan\theta}{2\sqrt{r_{\mathrm{core}}^2 - r_{\mathrm{min}}^2}}\,, \tag{9}$$

which can be rearranged to yield a value for ϵ instead:

$$\epsilon = \left(a_{\mathrm{tot}} - \frac{a}{\cos\theta}\right)\left(\frac{2\sqrt{r_{\mathrm{core}}^2 - r_{\mathrm{min}}^2}}{\tan\theta}\right)\,. \tag{10}$$

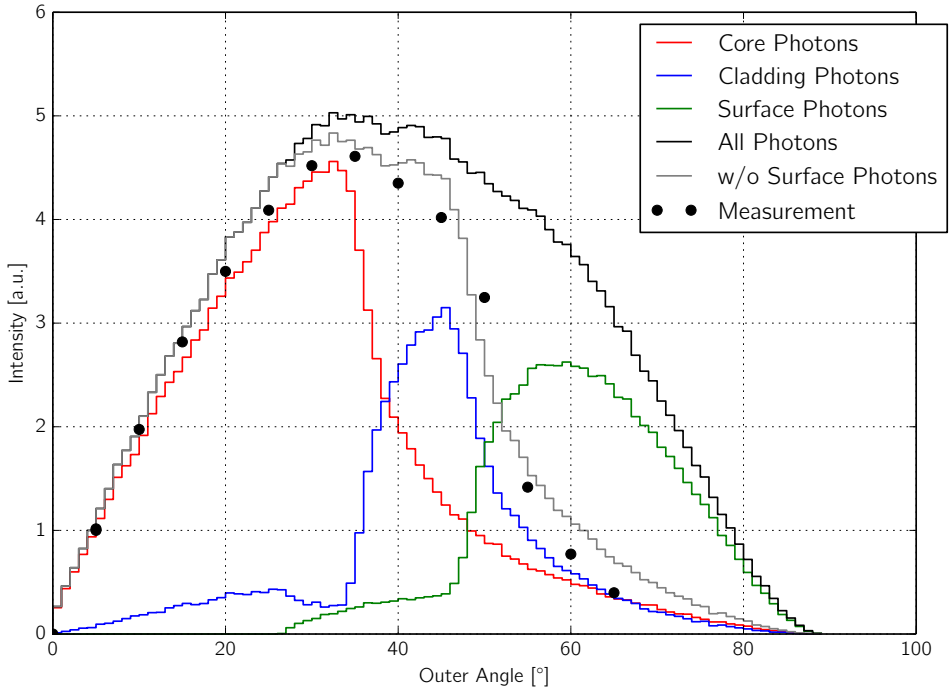

Figure 5: Angle dependent intensity for measurement and simulation data. The simulation data is shown broken down into its components of core, cladding and surface photons shown in red, blue and green respectively. The black line shows the total number of photons, while the grey line excludes surface photons.

The angle dependent values for ϵ, that are calculated using Eq. 10 for different wavelengths, are depicted in Fig. 9. It shows a linear increase up to an angle of 20°, where it starts to flatten. This general behaviour is also seen in Fig. 7, which leads to the assumption that the reflection loss coefficient is proportional to the interface angle of the photons. Above 20°, however, the calculated ϵ rises again while the average interface angle for core photons stays the same. Since Eq. 8 is only valid for core photons, the behaviour above 20° is not necessarily correct, since cladding photons influence the total attenuation coefficient at those angles. Even so, it can be used to roughly estimate the expected magnitude of the reflection loss coefficient for cladding photons. Figure 6 shows that the fraction of cladding photons rises at angles above 20°. If we assume that the total value of ϵ is an average of the different reflection loss coefficients of core and cladding photons, weighted by their number, the rising ϵ can be explained. This explanation requires the reflection loss coefficient at the cladding-cladding interface to be about three times bigger than at the core-cladding interface.
A wavelength dependency can be observed as well. The linear slope for small angles is present for all wavelengths, which leads to the assumption that the wavelength dependency

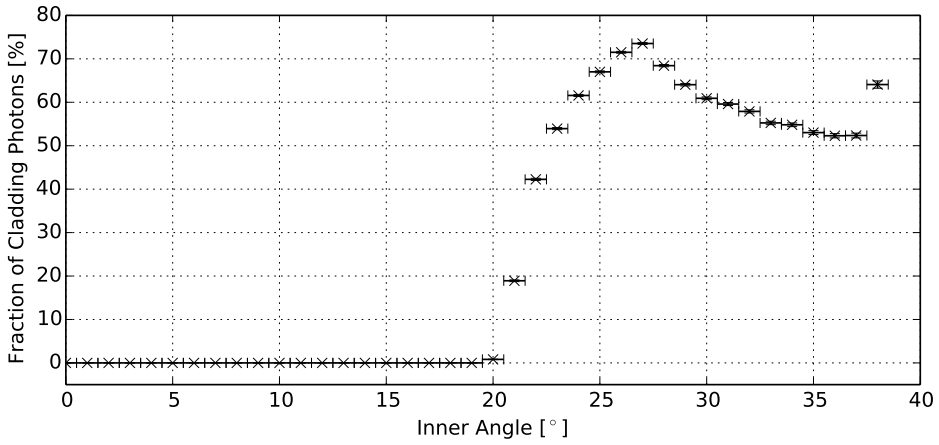

Figure 6: Percentage of cladding photons at various angles determined with the fibre simulation. [4]

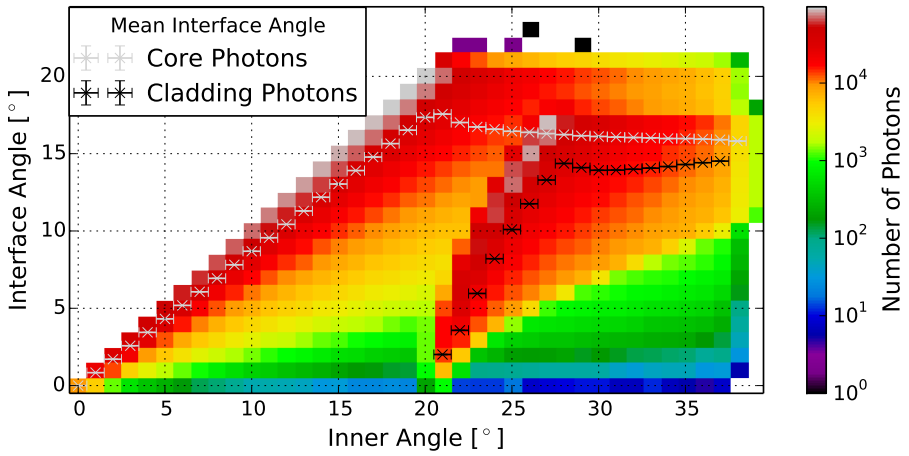

Figure 7: Histogram showing the interface angle depending on the angle inside the fibre. The average values for the interface angle are determined for every angle inside the fibre. The results are computed separately for core and cladding photons, but are shown superimposed in this image. [4]

is independent of the angular dependency:

$$\epsilon_{\mathrm{co}} = \epsilon(\lambda) \cdot \theta_{\mathrm{refl}} \,. \tag{11}$$

A value for $\epsilon(\lambda)$ is determined using measurement results from Ref. [4]. For low angles, a fit is performed with Eq. 9 for many different wavelengths, with a binning of 2 nm. In those fits, the value for the reflection loss coefficient is the only free variable. For r_{min}, the angle-dependent average value is used. The measurements and the fits over the data are depicted in Fig. 10, and the resulting coefficient is shown in Fig. 11, together with an

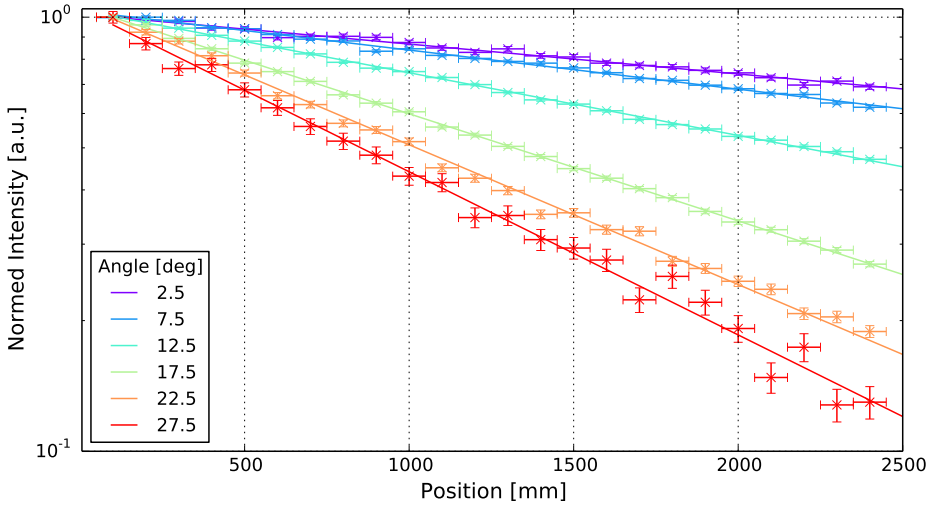

Figure 8: Normed light intensity for different positions of excitation obtained from simulation. The intensity decays exponentially with rising distance of the excitation point to the detector volume. Exponential functions are fitted to the data. The data points are averaged over all wavelengths.

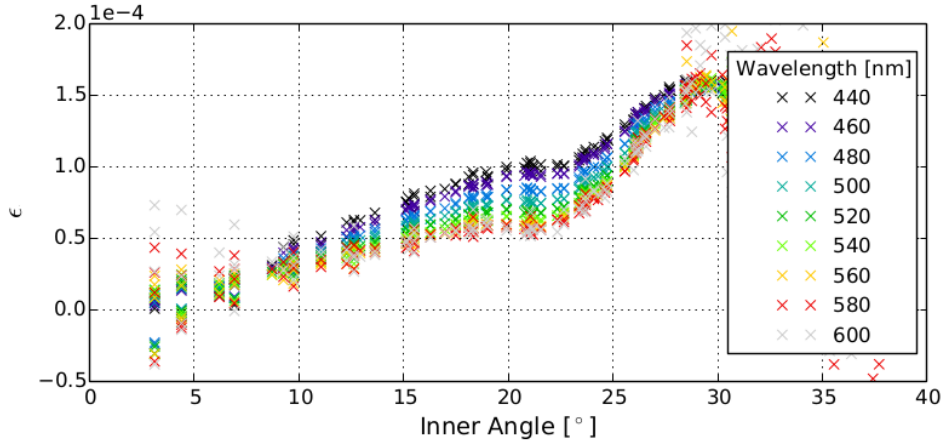

Figure 9: Calculated reflection loss coefficient ϵ at different angles for various wavelengths. [4]

exponential function of the form

$$a \cdot \exp(-(\lambda - 440) \cdot b) + c\,, \tag{12}$$

that was fitted to the results. The result of this fit for the six measured fibres are listed in Tab. 2 in the appendix.

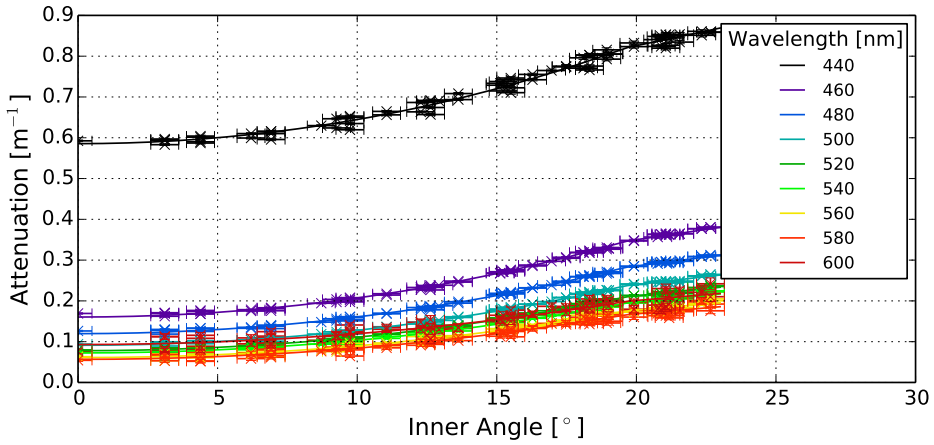

Figure 10: Angle dependent attenuation coefficient determined from measurements for various wavelengths. A fit is performed to obtain a value for the reflection loss coefficient ϵ at each wavelength. [4]

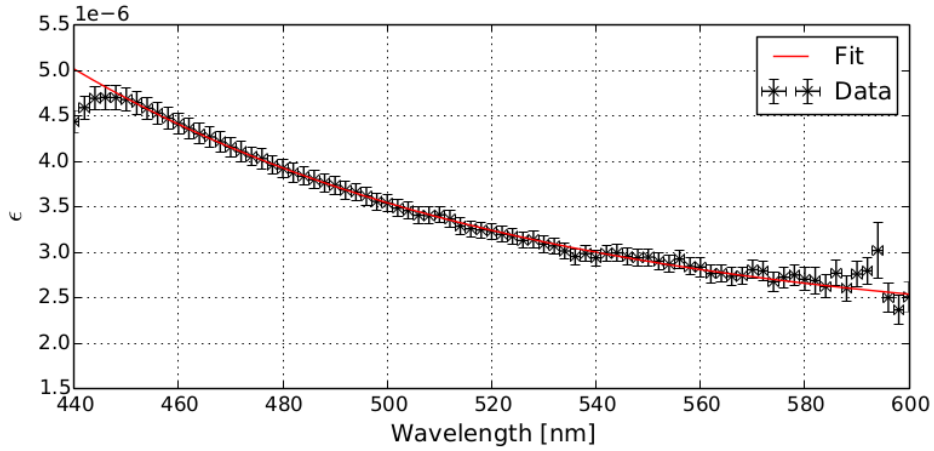

Figure 11: Wavelength dependency of the reflection coefficient ϵ. An exponential function has been fitted to the data. [4]

5 Conclusion

There are many mechanisms with which light can be lost during transmission through the fibre. The intrinsic absorption of the scintillator material and wavelength-shifter, Rayleigh scattering, radiation damage and fibre ageing are taken into account. They scale with the path length of the photons in the various materials. A function describing these loss mechanisms has been fitted to data gathered from fibre measurements. During production, the fibre quality of the main-series has improved compared with the pre-series so that an update of fibre parameters became necessary. A parameter describing the

additional attenuation coefficient due to impurities in the fibre material was reduced from $4.65 \times 10^{-2}\,\mathrm{m}^{-1}$ to $1 \times 10^{-2}\,\mathrm{m}^{-1}$.

In addition to the base attenuation, reflection losses at the material interfaces are considered as well. They scale with the number of reflections and are not implemented in the GEANT4 simulation directly, but are added during later analysis. Previously, the reflection loss coefficient was set to a constant value. It has been determined, however, that the reflection losses are different at each interface. Through simulation analysis and comparison to measurements, the angular dependence of the reflection loss coefficient is determined. For photons that move exclusively in the core material, the wavelength dependency of the reflection loss coefficient has been determined as well. Photons that interact with the fibre surface are not reflected at all, in contrast to simulation predictions. The necessary parameter files to run the simulation, as well as important equations used in the analysis are gathered in this note to aid with reproducibility.

6 Appendix

6.1 Calculation of Refractive Indices

Table 1: Values of parameters used in the Sellmeier equation (Eq. 1) to determine the wavelength-dependent refractive indices of fibre materials. Polystyrene composes the core, the inner cladding is made of PMMA (poly(methyl methacrylate)) and the outer cladding is assumed to be composed of PTFEMA (poly(trifluoroethyl methacrylate)). Data taken from Ref. [3].

Material	a	$b[\mathrm{nm}^2]$
Polystyrene	1.44355 ± 0.00099	20216 ± 211
PMMA	1.18188 ± 0.00066	11309 ± 181
PTFEMA	0.98323 ± 0.00012	9541 ± 15

6.2 Model for Cladding Photons

The derivation of this model and the definitions of all parameters can be found in Ref. [4]. The total path length in the fibre core L_{core}, the total path length in the cladding L_{clad}, the number of reflections N and the angle of photon path to the surface normal of the cladding-cladding interface γ_{cl} can be calculated. Input Variables:

- inner angle in degrees (θ)
- distance at closest approach to the fibre axis (r_{min})
- wavelength of the photon (wl)

Formulas:

$$\theta_{\text{refl}} = \arcsin\left(\sqrt{1 - \frac{r_{\text{min}}^2}{r_{\text{core}}^2}}\sin\theta\right)$$

$$b = \sqrt{r_{\text{core}}^2 - r_{\text{min}}^2}$$

$$x_{\text{co}} = \frac{b}{\tan\theta}$$

$$c = \sqrt{r_{\text{min}}^2 + x_{\text{co}}^2}$$

$$L_{\text{co}} = \sqrt{b^2 + x_{\text{co}}^2}$$

$$n_1 = \sqrt{1 + \frac{1.44355 \cdot wl^2}{wl^2 - 20216}}$$

$$n_2 = \sqrt{1 + \frac{1.181 \cdot wl^2}{wl^2 - 11309}}$$

$$\beta = \arcsin\left(\frac{L_{\text{co}}}{c}\cos\theta_{\text{refl}}\right)$$

$$\Gamma = \arcsin\left(\frac{n_1}{n_2}\cos(\theta_{\text{refl}})\right)$$

$$\alpha = \pi - \beta - \Gamma$$

$$\epsilon_{\text{angle}} = \arctan\left(\frac{r_{\text{min}}}{x_{\text{co}}}\right)$$

$$g = \frac{r_{\text{core}}\sin(\Gamma)}{\sin\alpha}$$

$$h = g\cos(\epsilon_{\text{angle}})$$

$$w = g\sin(\epsilon_{\text{angle}})$$

$$\Delta w = w - r_{\text{min}}$$

$$L_{\text{p}} = \sqrt{\Delta w^2 + b^2}$$

$$\phi = \arctan\left(\frac{\Delta w}{b}\right)$$

$$\lambda_{\text{angle}} = \arctan\left(\frac{h}{L_{\text{p}}}\right)$$

$$\psi = \arcsin\left(\frac{r_{\text{min}}}{r_{\text{core}}}\right)$$

$$\eta = \arcsin\left(\frac{r_{\text{core}}}{r_{\text{clad}}}\sin(\pi - \psi - \phi)\right)$$

$$\tau = \psi + \phi - \eta$$
$$\rho = \frac{\pi}{2} - \lambda_{\text{angle}}$$
$$q = \frac{r_{\text{clad}} \sin(\tau)}{\sin(\pi - \phi - \psi)}$$
$$L_{\text{cl}} = \frac{q}{\cos(\lambda_{\text{angle}})}$$
$$x_{\text{cl}} = L_{\text{cl}} \sin(\lambda_{\text{angle}})$$
$$\bar{x} = x_{\text{cl}} + x_{\text{co}}$$
$$L_{\text{core}} = \frac{L_{\text{co}}}{\bar{x}}$$
$$L_{\text{clad}} = \frac{L_{\text{cl}}}{\bar{x}}$$
$$\gamma_{\text{cl}} = \arccos(\cos(\eta)\cos(\rho))$$

The number of reflections N are

$$N = \frac{x}{\bar{x}},$$

where x is the distance from excitation point to the fibre end.

6.3 Input Parameter Files

In the following section, all parameters that need to be provided to the simulation via a parameter file are listed for simulations used in Ref. [4].

parameters.dat

- Fibre Length: 2.5
- Semi-axis y: 0.125
- Semi-axis z: 0.125
- Probability to lose photons at fibre surface: 1
- Mirror placement at fibre end: 1
- Mirror reflectivity: 0.7
- Detector material, vacuum/polystyrene (0/1): 0
- Scintillation emission spectrum: "parameters/ScintEmission/p-Terphenyl_emission.csv"
- Number of interpolated points per emission spectrum interval: 4

- WLS absorption spectrum: "parameters/WLSAbsorption/TPBD_absorption_1000ppm.csv"
- WLS emission spectrum: "parameters/WLSEmission/TPBD_emission.csv"
- Scintillation yield: 4.45
- Resolution scale: 5.5
- Fast decay time: 1.2
- Slow decay time: 1.2
- Yield ratio: 0.8
- Birks constant: 0.126
- WLS decay time: 2.8
- Refractive index of vacuum: 1
- Refractive index of fibre core: sqrt(1. + 1.44355*x*x / (x*x - 20216.))
- Refractive index of inner cladding: sqrt(1. + 1.18188*x*x / (x*x - 11309.))
- Refractive index of outer cladding: sqrt(1. + 0.98323*x*x / (x*x - 9541.))
- Absorption in fibre core: 7.9e-10*exp(6.715*1239.842/x) + 3.143e-5*TMath::Voigt(1.0/x-1.403e-3,0.816e-5,1.389e-5) + 0.466e-5*TMath::Voigt(1.0/x-1.644e-3,0.975e-5,1.389e-5) + 0.191*0.466e-5*TMath::Voigt(1.0/x-1.872e-3,0.975e-5,1.389e-5) + 1.628e-5*TMath::Voigt(1.0/x-1.321e-3,1.473e-5,1.389e-5) + 0.102e-5*TMath::Voigt(1.0/x-1.548e-3,0.986e-5,1.389e-5) + 0.191*0.102e-5*TMath::Voigt(1.0/x-1.762e-3,0.986e-5,1.389e-5)
- Absorption in inner cladding: 119./100.*104./105.*8./3.* (1.628e-5*TMath::Voigt(1.0/x-1.321e-3,1.473e-5,1.389e-5) + 0.102e-5*TMath::Voigt(1.0/x-1.548e-3,0.986e-5,1.389e-5) + 0.191*0.102e-5*TMath::Voigt(1.0/x-1.762e-3,0.986e-5,1.389e-5))
- Absorption in outer cladding: 143./168.*104./105.*7./3.* (1.628e-5*TMath::Voigt(1.0/x-1.321e-3,1.473e-5,1.389e-5) + 0.102e-5*TMath::Voigt(1.0/x-1.548e-3,0.986e-5,1.389e-5) + 0.191*0.102e-5*TMath::Voigt(1.0/x-1.762e-3,0.986e-5,1.389e-5))
- Absorption in fibre core due to irradiation: (x<=400)*0.40*pow(y,0.8)*exp(-3.01E-2*(400-450)) + (x>400)*0.40*pow(y,0.8)*exp(-3.01E-2*(x-450))

- Absorption in inner cladding due to irradiation: (exp(10.6422-0.0303786*x)*1. + (1.34305*TMath::Gaus(x,422.81,27.474)+exp(15.5921-0.0406339*x)+exp(4.4398 -0.0117956*x))*0.)*y
- Absorption in outer cladding due to irradiation: (exp(10.6422-0.0303786*x)*1. + (1.34305*TMath::Gaus(x,422.81,27.474)+exp(15.5921-0.0406339*x)+exp(4.4398 -0.0117956*x))*0.)*y
- Sections file: parameters/RadMap/noRad.txt
- Rayleigh scattering strength in fibre core: 8./27.*TMath::Pi()*TMath::Pi()* TMath::Pi()/x/x/x/x*1e36*pow(1.44355*x*x / (x*x - 20216.),2)*pow(3 + 1.44355*x*x / (x*x - 20216.),2)*1.3806488e-23*295.*5.8e-10*4.010
- Rayleigh scattering strength in inner cladding: 8./27.*TMath::Pi()*TMath::Pi()*TMath::Pi()/x/x/x/x*1e36*pow(1.18188*x*x / (x*x - 11309.),2)*pow(3 + 1.18188*x*x / (x*x - 11309.),2)*1.3806488e-23*295.*5.2e-10*1.1
- Rayleigh scattering strength in outer cladding: 8./27.*TMath::Pi()*TMath::Pi()*TMath::Pi()/x/x/x/x*1e36*pow(0.98323*x*x / (x*x - 9541.),2)*pow(3 + 0.98323*x*x / (x*x - 9541.),2)*1.3806488e-23*295.*5.2e-10*1.1

p-Terphenyl_emission.csv

```
1.9     0
2.0     0
2.1     0
2.2     0
2.3     0
2.4     0
2.5     0
2.6     0
2.7     0
2.831   0
2.939   2
3.063   5
3.186   13
3.310   29
3.449   58
3.527   69
3.559   71
3.607   87
3.629   95
```

3.654	100
3.683	95
3.755	71
3.805	79
3.867	53
3.932	16
4.058	0
4.1	0
4.2	0
4.3	0
4.4275	0

TPBD_absorption_1000ppm.csv

1.900	1.25E+17
1.925	2.77E+16
1.950	6.38E+15
1.975	1.53E+15
2.000	3.78E+14
2.025	9.69E+13
2.050	2.57E+13
2.075	7.03E+12
2.100	1.99E+12
2.125	5.78E+11
2.150	1.73E+11
2.175	5.32E+10
2.200	1.68E+10
2.225	5.45E+9
2.250	1.81E+9
2.275	6.18E+8
2.300	2.16E+8
2.333	5.56E+7
2.367	1.43E+7
2.400	3.97E+6
2.433	1.14E+6
2.467	3.28E+5
2.500	1.01E+5
2.533	3.20E+4
2.567	1.01E+4
2.600	3.39E+3
2.633	1.17E+3
2.667	4.03E+2
2.700	1.47E+2
2.733	5.48E+1
2.767	2.03E+1
2.800	7.96E+0
2.833	3.18E+0
2.867	1.26E+0
2.900	5.27E−1
2.933	2.24E−1

2.967	9.47E–2
3.000	4.18E–2
3.020	2.57E–2
3.040	1.59E–2
3.0729	4.60E–3
3.0934	3.68E–3
3.1120	2.94E–3
3.1368	1.84E–3
3.1616	1.04E–3
3.1864	6.13E–4
3.2112	3.89E–4
3.2360	2.62E–4
3.2608	1.84E–4
3.2856	1.32E–4
3.3166	9.49E–5
3.3476	7.50E–5
3.4096	5.62E–5
3.4716	4.62E–5
3.5335	4.08E–5
3.5807	3.95E–5
3.5955	3.96E–5
3.6575	4.13E–5
3.7195	4.42E–5
3.7815	5.05E–5
3.9055	7.07E–5
4.0295	1.10E–4
4.1535	1.71E–4
4.2775	2.50E–4
4.4014	3.09E–4
4.4275	3.13E–4

TPBD_emission.csv

1.9	0
1.922	17
2.046	58
2.170	141
2.294	307
2.418	557
2.542	831
2.591	911
2.641	968
2.678	990
2.715	999
2.765	962
2.814	891
2.914	665
3.038	333
3.100	187
3.162	76

```
3.224    19
3.286    0
3.4      0
3.5      0
3.6      0
3.7      0
3.8      0
3.9      0
4.0      0
4.1      0
4.2      0
4.3      0
4.4275   0
```

noRad.txt

```
1
0  0
```

6.4 Wavelength Dependency of the Reflection Coefficient

Table 2: Parameters for the exponential function fitted to the wavelength dependent reflection loss coefficient in the core material. The fits were performed in the scope of Ref. [4].

Fibre	$a \times 10^{-6}$	b [nm^{-1}]$\times 10^{-2}$	$c \times 10^{-6}$
1	3.28 ± 0.04	1.15 ± 0.04	3.19 ± 0.05
2	3.43 ± 0.02	1.27 ± 0.03	2.80 ± 0.03
3	3.26 ± 0.04	1.04 ± 0.03	2.48 ± 0.05
4	3.04 ± 0.06	1.00 ± 0.04	2.43 ± 0.07
5	2.62 ± 0.07	1.16 ± 0.09	2.08 ± 0.09
6	3.33 ± 0.05	1.31 ± 0.06	2.16 ± 0.06

References

[1] LHCb collaboration, *LHCb Tracker Upgrade Technical Design Report*, CERN-LHCC-2014-001. LHCb-TDR-015.

[2] A. B. R. Cavalcante *et al.*, *Refining and testing 12,000 km of scintillating plastic fibre for the LHCb SciFi tracker*, October 2018.

[3] M. Deckenhoff, *Scintillating Fibre and Silicon Photomultiplier Studies for the LHCb Upgrade*, PhD thesis, TU Dortmund, 2015, CERN-THESIS-2015-318.

[4] R. Manderfeld, *Study of the angle-dependent attenuation length of scintillating fibres for the LHCb SciFi Tracker*, Master's thesis, TU Dortmund, 2018.

[5] R. Ekelhof, *Studies for the LHCb SciFi Tracker – Development of modules from scintillating fibres and tests of their radiation hardness*, PhD thesis, TU Dortmund, 2016, CERN-THESIS-2017-098.

[6] M. Deckenhoff, *Simulation of Scintillating Fibres in Geant4*, LHCb-PUB-2014-023.

[7] J. Surmann and R. J. Ekelhof, *Simulating the Properties of Scintillating Fibres - The influence of angles and track lengths of photons on the absorption*, LHCb-INT-2016-009.